applied sciences

MDPI

Article

Geomechanical Analysis of the Main Roof Deformation in Room-and-Pillar Ore Mining Systems in Relation to Real Induced Seismicity

Dariusz Chlebowski * and Zbigniew Burtan

Faculty of Civil Engineering and Resource Management, AGH University of Krakow, Mickiewicza 30 Av., 30-059 Cracow, Poland

* Correspondence: chlebo@agh.edu.pl

Abstract: Rockbursts represent one of the most serious and severe natural hazards emerging in underground copper mines within the Legnica–Glogow Copper District (LGCD) in Poland. The contributing factor determining the scale of this event is mining-induced seismicity of the rock strata. Extensive expertise of the copper mining practitioners clearly indicates that high-energy tremors are the consequence of tectonic disturbances or can be attributed to stress/strain behaviour within the burst-prone roof strata. Apparently, seismic activity is a triggering factor; hence, attempts are made by mine operators to mitigate and control that risk. Underlying the effective rockburst control strategy is a reliable seismicity forecast, taking into account the causes of the registered phenomena. The paper summarises the geomechanics analyses aimed to verify the actual seismic and rockburst hazard levels in one of the panels within the copper mine Rudna (LGCD). Two traverses were designated at the face range and comparative analyses were conducted to establish correlations between the locations of epicentres of registered tremors and anomaly zones obtained via analytical modelling of changes in stress/strain behaviours within the rock strata. The main objective of this study was to evaluate the likelihood of activating carbonate/anhydrite layers within the main roof over the excavation being mined, with an aim to verify the potential causes and conditions which might have triggered the registered high-energy events. Special attention is given to two seismic events giving rise to rockbursts in mine workings. Results seem to confirm the adequacy and effectiveness of solutions provided by mechanics of deformable bodies in the context of forecasting the scale and risk of dynamic phenomena and selecting the appropriate mitigation and control measures in copper mines employing the room-and-pillar mining system.

Keywords: underground mining; rock mechanics; mining tremors; rockburst hazard

check for updates

Citation: Chlebowski, D.; Burtan, Z. Geomechanical Analysis of the Main Roof Deformation in Room-and-Pillar Ore Mining Systems in Relation to Real Induced Seismicity. *Appl. Sci.* **2024**, *14*, 5710. https://doi.org/10.3390/app14135710

Academic Editor: Fabrizio Balsamo

Received: 5 May 2024
Revised: 14 June 2024
Accepted: 27 June 2024
Published: 29 June 2024

Copyright: © 2024 by the authors. Licensee MDPI, Basel, Switzerland. This article is an open access article distributed under the terms and conditions of the Creative Commons Attribution (CC BY) license (https://creativecommons.org/licenses/by/4.0/).

1. Introduction

Mining-induced seismicity in rock strata and associated rockbursts represent the most perilous potential hazards facing the copper and coal mine operators in Poland. Since the geology of rock strata, rock properties and mining conditions in the Legnica–Glogow Copper District (LGCD) [1,2] differ from those prevailing in the Upper Silesia Copper Basin (USCB) [3,4], the scale and nature of rockburst hazard manifestations should be different, too. Nevertheless, whether mineral or metal is being mined, the underlying cause, mechanism and origins of the registered events are basically the same. Tremors occur due to forces acting upon the structure of the rock strata and triggering the occurrence of dynamic phenomena, revealed by the release of seismic energy. In consideration of the location of these phenomena and the nature of cause-and-effect relationships, two types of mining tremors can be distinguished [5]. The first group includes mining-induced seismic events, their foci located in the vicinity of the deposit, in the immediate or main roof strata [6,7]. In the case of those tremors, the parameters of the mining operations and the local geological settings are major determinants of the scale, spatial distribution and energy

levels of registered seismicity. The other group includes tremors that are only partly related to the ongoing underground mining operations and should be attributed to local changes within the extensive mining sites due to progressing mining operations in combination with the presence of tectonic disturbances [8,9]. Those are mostly high-energy tremors whose foci are mostly located at a considerable distance from the active excavations.

Despite the continuing development of monitoring equipment, tools and systems, the state-of-the-art and practice in the field of seismic hazard forecasting is still far from satisfactory. This issue is of particular interest for mining engineers, mining companies as well as research and development units [10]. As seismic events can potentially produce most adverse impacts, leading to rockbursts or rock de-stressing in excavations, and work safety has been considered the top priority, new methods of predicting mining-induced seismicity are being sought and existing methods are being upgraded [11,12]. In order to improve the effectiveness and reliability of seismicity forecasts, diverse criteria and concepts are recalled, including the solutions offered by mining engineering, geophysics and geomechanics. Among well-known solutions are those based on correlations between seismicity data and registered roof convergence values and changes of the drillhole diameter in the roof strata [13,14]. There are methods of seismic risk assessment that involve the detailed analysis of the attributes of registered events [15,16], such as times series of seismic and seismoacoustic energy emissions, taking into account the local geological settings and mining conditions [17–19]. The interpreting criteria based on analyses of focal mechanisms [20–22] and those recalling the Gutenberg–Richter law are being developed and upgraded [23–25]. A large group of methods for mining-induced seismicity evaluation use the P-wave and S-wave tomography profiles to identify anomaly zones [25–27] or rely on peak particle velocity (PPV) measurements in the vicinity of mining excavations [28,29]. Probabilistic models are now widely applied [30,31] alongside machine learning methods [32,33]. Generally, predictions by geomechanical methods consist of observations of the changes in the stress–strain behaviour or elastic energy with an aim to identify the zones where the conditions are likely to trigger the dynamic processes leading to disruption (failure) of the rock strata [34–37].

The study explores the applications of geomechanical strain and energy forecasts based on analytical simulations in terms of evaluating the seismic and rockburst hazard levels in underground mining. The case study recalled is that of the panels being mined (XVII/1) in the copper mine Rudna, operated by the KGHM Polska Miedź SA corporation (LGCD). The geological and mining conditions are summarised, followed by the quantitative energy analysis of seismic events registered over a 6-year period, starting from the moment when the mining operations in this site were initiated. Within the considered period, several dynamic events were registered, including rockbursts and rock de-stressing events. Two of these rockbursts (registered in December in Year 3 and in Year 6) were regarded as untypical in terms of their extent and scale of impacts they exerted. Within the considered panel, two traverse sections were designated, emulating the status of mining operations as of the day when the two previously mentioned rockbursts were registered. Within the designed areas (traverses), the back-analysis was conducted to compare the locations of registered tremor epicentres and zones of anomalous changes in elastic strain energy density and the effort factor obtained by analytical modelling. The vertical coordinate of the hypocentre of events leading to the two rockbursts obtained by recalling the geophysical foci mechanism was found to be 100 m above the deposit; that is why the changes in the stress–strain behaviour were observed mostly in the horizon of carbonate and anhydrite formations (fully in line with the lithographical profile of the site). The objective of the analysis was to evaluate the potentials of activating the burst-prone layers within the main roof strata to establish the origins and causes of registered high-energy seismicity, with the main focus on phenomena leading to rockburst events. In a broader perspective, the objective was to verify the applicability and effectiveness of solutions offered by mechanics of deformable media [38–43] having relevance to the following:

– Forecasting the mining-induced processes within the rock strata;

– Steering the elements of the room-and-pillar mining systems such as to reduce the rockburst and seismic hazard levels.

Most forecasts of mining-induced seismicity in coal mining in Poland rely on the solutions offered by the 3D theory of elasticity with the boundary conditions in terms of displacement, as proposed by F. Dymek [38] or by H. Gil [39]. Another approach, based on the cylindrical plate bending or the theory of pressure waves, was proposed by W. Budryk [41] or H. Sałustowicz [40,42]. In this study, the definition of the state of displacement and strain in the copper deposit within the Zechstein layers (LGCD) is based on algorithms derived according to geometrical-integral theory of mining impacts, advanced by S. Knothe and W. Budryk [43].

2. Materials and Methods

2.1. Geological and Mining Conditions in the Area

The copper deposit formed in the bed-like structure found within the panel XVII/1 in the copper mine Rudna comprises light-grey sandstones in the Rotliegend rock, and lower Zechstein copper-bearing shales and dolomites (Figure 1). Along the principal NW-SE direction coincident with the bed extension range, there is a sedimentation-type field of geological disturbances in the form of white sandstone roof elevation. In the vicinity of this disturbance, the thickness of the copper-bearing shale layer is decreasing and finally disappears. At the same time, the mineralisation profile across the layer is altered. On the slope of the bed elevation, sandstone layers with illite–anhydrite binders, up to 5 m in thickness, are found locally in the roof of sandy formations. The bed thickness in the south-west section varies from 4 to 8 m and then increases to 13 m in the northern part, subsequently going down to 6–7 m along the direction coinciding with that determined by the presence of old excavations in this area.

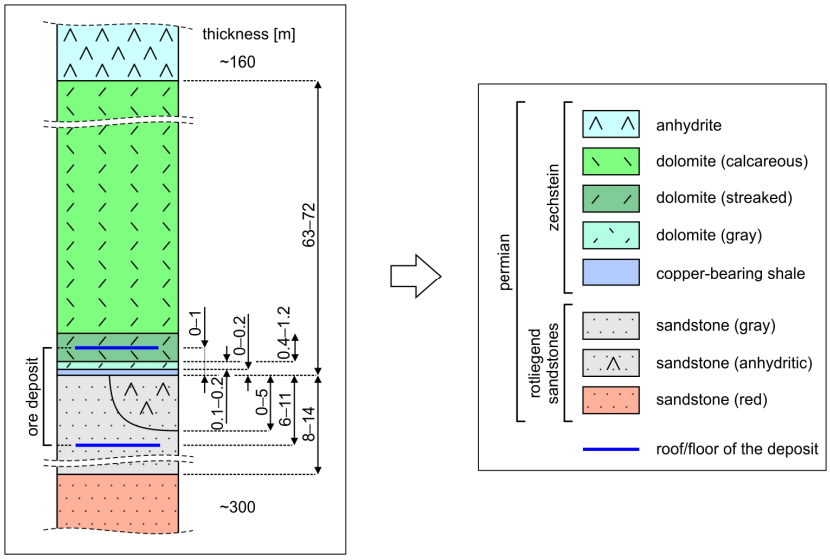


Figure 1. A part of lithological profile in the vicinity of the ore deposit (XVII/1 site).

The deposit lies at the depth of about 1050 m, dipping at 2–6° in the NE direction; however, in the elevation zone, the ascending vertical angle tends to vary considerably. In the roof strata where the shale is found, there is some dark-grey sandy striped dolomite with few anhydrite inclusions. In the shale-free section, the roof adjoins more compact grey-coloured limestone dolomite with anhydrite and gypsum inclusions. The total thickness of the carbonate-shale layer in the considered section varies from 72 to 96 m; it is overlain by a 160 m thick anhydrite layer. The floor comprises light-grey, fine-grained quartzite sandstone with an illite binder, 8–14 m in thickness, with the increasing depth gradually replaced by medium-grained red-coloured sandstone, about 300 m in thickness (Figure 1).

Within the panel, there are discontinuities and dislocations in the form of major faults (70–90°) oriented in the NW-SE and NE-SW direction, with the downthrow of 0.1–4.4 m. There are also some vertical and inclined roof fractures, oriented mainly in the NE-SW (25–35°) and NW-SE (295–305°) direction.

Geomechanical properties of the rock strata in the investigated area were determined through the geotechnical analyses of rock samples from several boreholes. The variability range of basic rock parameters in the face entry drivage and in the immediate roof and floor layers is shown in Table 1.

Table 1. Geomechanical parameters of rock layers (XVII/1 site).

Rock Layer	Rc [MPa]	Es [GPa]	ν [–]
Roof (25 m rock package)	108.9–129.2	33.5–59.1	0.15–0.28
Orebody zone	57.8–77.6	16.7–19.0	0.13–0.24
Floor (6 m rock package)	21.3–26.5	10.0–16.4	0.12–0.18

Panel XVII/1 is located in the central part of the mined area in the Rudna mine. According to plans, the mining operations started at the boundary with the adjacent panel XVI/1, advancing on the strike. The face of panelling operations 550–850 m in length advanced along the cluster of galleries T-236/236a (on the right-hand side) and the abandoned excavations (on the left-hand side), in the direction of the descending gallery U5/8. Because of the varied thickness of the commercial deposit, three versions of room-and-pillar stoping methods were employed, designated as R-UO (to mine beds up to 7 m in thickness, with roof deflection), RG-6 (to mine beds up to 15 m in thickness, with rock filling) and RG-8/9 (to mine beds up to 15 m, with sand filling). Due to a locally elevated risk of roof caving, in Year 3 and Year 4, two face advance operations were employed: the main stoping over the distance of ~700 m (advancing on the strike) and supplementary operations over the distance ~480 m (advancing to the rise). The sketches below illustrate the state of mining operations within panel XVII/1 in the 3-year time interval: at the end of Year 3 (Figure 2) and the at end of Year 6 (Figure 3).

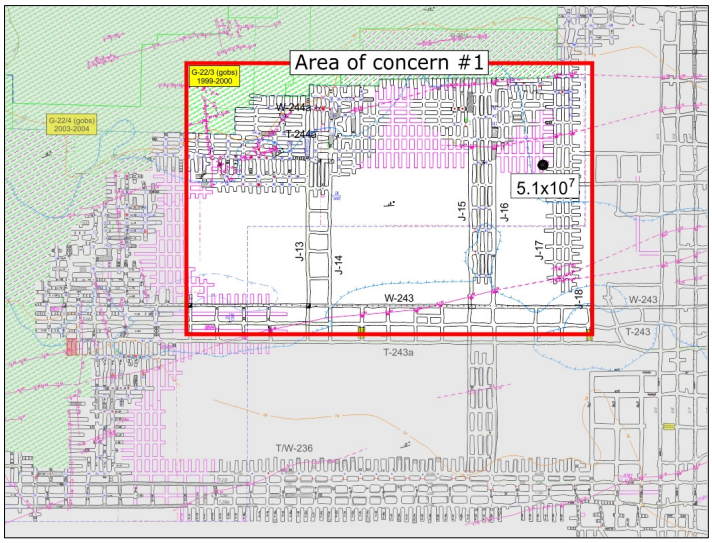


Figure 2. Status of mining operations in panel XVII/1 at the end of Year 3.

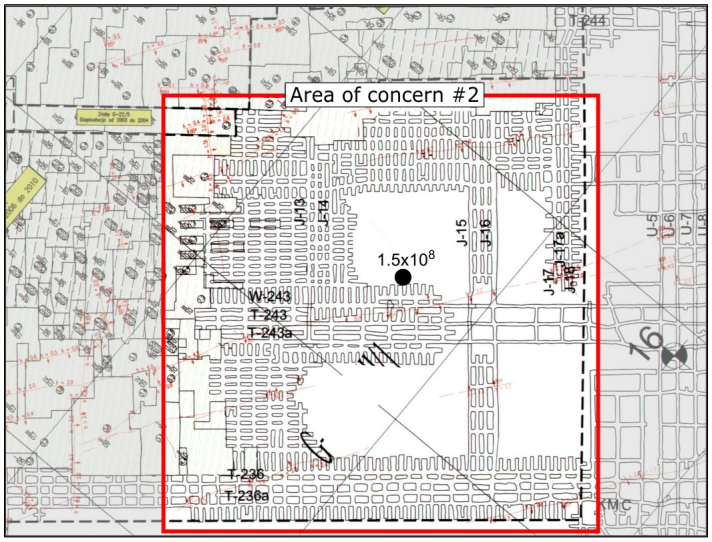


Figure 3. Status of mining operations in panel XVII/1 at the end of Year 6.

The indicated time intervals are by no means arbitrarily chosen. Actually, they are associated with high-energy seismic events registered in December in Year 3 and in Year 6, leading to major rockbursts in mining excavations. These particular events were selected for the analysis because they were considered atypical in the conditions prevailing in the LGCD copper district in terms of the contributing factors and the nature of impacts they exerted. A general characteristic of mining-induced seismicity and the rockburst hazard conditions is given in Section 2.2.

In the context of further mining operations and to select the adequate rockburst control strategy, the back analysis of geomechanical behaviour was performed to reveal the potential causes of the registered seismic events triggering the rockbursts. Hence, traverses are indicated on the maps of the excavations (Figures 2 and 3) with a thick red line (area of concern #1—Figure 2, area of concern #2—Figure 3) which were subject to rigorous geomechanical analyses.

2.2. General Characteristic of Seismic Activity and Rockburst Hazard

In the first 6 years of mining operations in the panel XVII/1, seismic activity expressed as the number of seismic events (ΣN), total energy level (ΣE) and seismic energy per a single high-energy tremor ($\Sigma E_w/N_w$) (Table 2) was variable. In the investigated period, the total number of registered events with energy $\geq 10^3$ J was 1504, equivalent to the total energy expense of 1.45×10^9 J. While the overall seismic activity remained in the low- and medium-energy range, still 16.3% of the entire population of tremors were high-energy events ($\geq 10^5$ J) (254, year average ~41/year), accounting for 99.2% of total seismic energy released from the rock strata (1.43×10^9 J, year average ~2.38×10^8 J/year).

The distribution of seismic events in the function of released energy (Figure 4) can be expressed by an exponential dependence with a relatively good fit ($R^2 = 0.965$) and the general criteria of the Gutenber–Richter distribution are satisfied. It is of primary importance considering the random nature of events and the ability of the rock strata to release large amounts of energy; hence, the likelihood of triggering a high-energy event tend to decrease sharply, yet the probability of a tremor occurrence still cannot be assumed to be almost non-existent.

Considering the number of seismic events, it is reasonable to assume that even though the probability of its occurrence remains low, a high-energy event is bound to occur after a certain time. From the standpoint of mining practice, it will occur after the working face advanced over a specified distance.

Table 2. Mining-induced seismicity in panel XVII/1 (in the first six years).

Year	10^3 J	10^4 J	10^5 J	10^6 J	10^7 J	10^8 J	ΣN [–]	ΣE [J]	$\Sigma E_w/N_w$ [J]
1st	15	10	6	2	1	1	35	2.63×10^8	2.62×10^7
2nd	96	40	19	10	4	--	169	1.25×10^8	3.73×10^6
3rd	164	62	36	13	7	1	283	3.46×10^8	6.04×10^6
4th	234	87	30	18	3	--	372	1.58×10^8	3.04×10^6
5th	241	92	39	15	9	--	396	2.70×10^8	4.22×10^6
6th	162	56	20	5	5	1	249	2.91×10^8	9.32×10^6
Σ/av.	912	347	150	63	29	3	1504	1.45×10^9	5.89×10^6

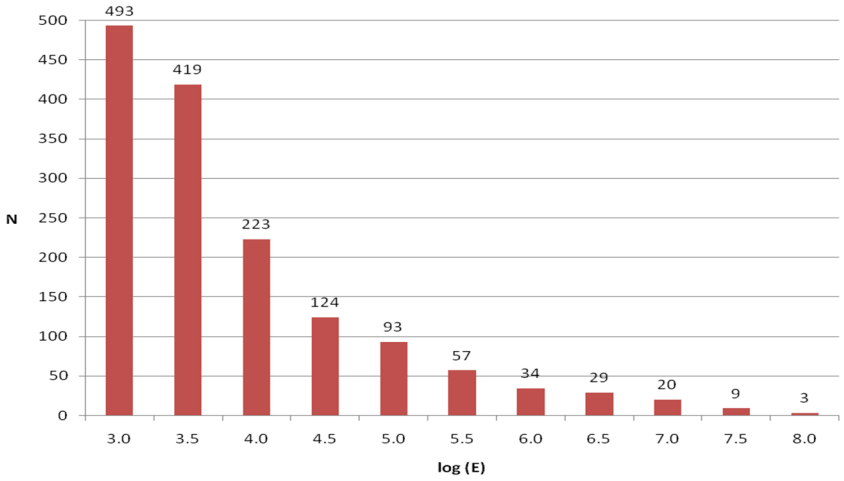


Figure 4. Number of seismic events in the energy class ($\geq 10^3$ J).

In relation to the progress of mining operations, the level of seismicity expressed by a number of registered events was steadily increasing (except for Year 6), both in terms of high-energy tremors and the entire population of events ($\geq 10^3$ J). In consideration of the energy class, a cyclic nature of seismic activity can be observed and events in the energy range 10^7–10^8 J occur regularly, which affects the total value of seismic energy release and the average energy release per one event. Insofar as this cyclicity can be attributed to mining activities, the occurrence of high-energy tremors is indicative of the uniform yet random nature of such events even though the energy might be released during weaker tremors.

The foci of registered seismic events (including high-energy tremors) are concentrated in the centre of the panel, though some of them appear to be correlated with the locations of faulting zones (Figure 5). In regard to the foci locations with respect to the working face advance, it is reasonable to conclude that the majority of tremors were registered in the undisturbed strata, prior to the panelling operations; those registered in old abandoned excavations were a minority.

In the analysed 6-year period of continuing mining operations in panel XVII/1, 7 rockbursts and rock de-stressing events were registered in the excavations, differing in magnitude and impacts they exerted. All these events were triggered by high-energy tremors whose foci were located mostly near the boundary of the old excavations, along the panelling line or in the vicinity of tectonic disturbances with diverse profiles and faults with the downthrow not exceeding the height of the face entry drivage. Analyses conducted within the scope of the present study have relevance to the conditions prevailing after the occurrence of two rockbursts registered in December in Year 3 triggered by tremors of 5.1×10^7 J and 1.3×10^6 J (Figures 2 and 5), followed by one rockburst event registered in December in Year 6, triggered by a tremor with magnitude 1.5×10^8 J (Figures 3 and 5). The reason why these particular events were selected for further analysis can be explained

by specific conditions of their occurrence and the unusual nature and scale of impacts, offering us a better insight into the issue. In both cases, the impacts would be revealed as floor upheaving, sidewalls sliding and stope failure or fracturing of the immediate roof, yet the scale and scope of impacts produced by the rockburst in Year 3 seem disproportionately high in relation to the seismic energy of triggering tremors. That the impacts were really extensive is evidenced by the amount of 41,000 Mg of ore produced without any blasting while implementing the mitigation measures and restoring the normal operations in the mine workings. In regard to the event registered in December in Year 6, its impacts were regarded as proportional to the tremor energy (in the conditions prevailing in LGCD), yet in this case the epicentre was located nearby the fault with the downthrow of 3–5 m, traversing the panel diagonally, this aspect merited a thorough analysis.

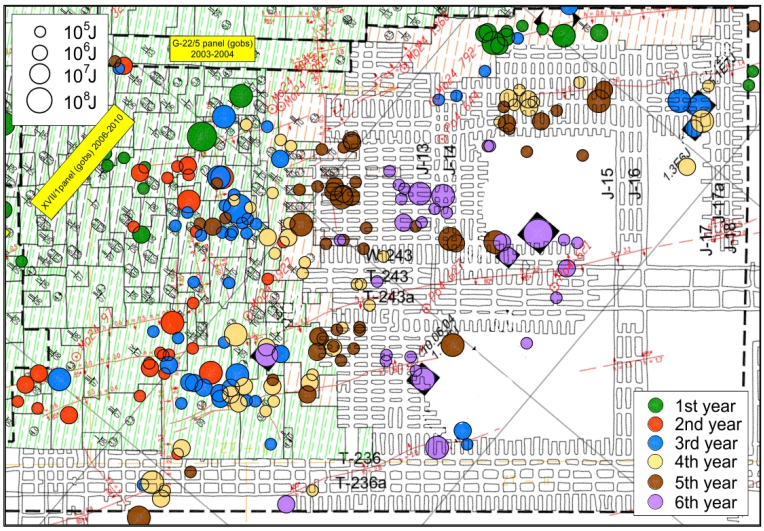


Figure 5. Foci locations during tremors in the energy class $\geq 10^5$ J.

In regard to mining-induced seismicity in all mines within the LGCD copper district, there appears to be a straightforward relationship between the number of seismic events and the number of impact-exerting events: the higher the energy of the seismic event, the larger the probability that a rockburst/rock de-stressing should occur. Statistics compiled over the 6 years of mining operations reveal that seismic events exerting serious impacts (rockbursts and de-stressing events) would be triggered by tremors of 10^6 J (~2%), tremors in the energy class 10^7 J (~21%), tremors in the class 10^8 J (~87%) and, finally, tremors of 10^9 J (100%). Considering the previous mining-induced seismicity (Table 2) and mining and geological conditions in the panel XVII/1 (Figure 3), it is unreasonable to expect a decrease in seismic activity while mining operations continue, and the occurrence of an event exerting serious impacts cannot be precluded whilst the current mining methods and technologies are still employed. That this hypothesis is true is evidenced by high rockburst risk levels subsisting during mining operations in the neighbouring panels XVII/2, XVII/3, XVI/1 and XVI/2, associated with high-energy seismicity.

2.3. Assumptions for the Analytical Assessment of Tremor-Prone Formations Activation Possibility

Mining practice in the LGCD copper district reveals that in the majority of cases, the high-energy mining-induced seismicity can be attributable to faulting or to roof failures in burst-prone strata with high strength parameters. In the case of the two considered rockburst events (registered at the end of Year 3 and at the end of Year 6), the vertical coordinates of epicentres of triggering events were found to be of the order of 100–130 m above the floor horizon. Thus, taking into account the geological settings in the area (Figure 1), the hypothesis underlying the present analysis was formed, stating that the analysed seismic events with the energy class 5.1×10^7 J and 1.5×10^8 J were triggered by

rock fracturing in the vicinity of anhydrite and carbonate layers. The epicentre of the tremor attributed to the second burst (registered at the end of Year 6) located in the vicinity of a fault, and thus, it is reasonable to conclude that the presence of tectonic disturbances has the potential of triggering seismic events whilst the released energy is likely to exceed 10^5 J. Analysing the advance of mining operations and considering mining-induced seismicity, still no straightforward relationship can be established between the mining conditions and locations of faults which reliably determine the occurrence of high-energy tremors. The actual position of the advancing face in the vicinity of tectonic disturbances cannot be treated as the only factor sufficient to trigger tremors which appear to be random phenomena, unrelated to the mining and geological conditions. Actually, variable and locally unpredictable parameters of the rock strata ought to be regarded as random factors as well. Extensive studies have shown that while the mining operations advanced, the working face often became close to the zone of tectonic disturbances yet no high-energy events would be triggered whilst the energy was released in the form of weaker tremors. It appears that it is only when the rock strata are not able to release the energy through weaker tremors and large amounts of energy are thus accumulated, the risk of a high-energy seismic event should increase.

The level of low-energy and medium-energy seismic activity in panel XVII/1 can be regarded as moderate in the conditions of the LGCD copper district. Hence, no premises seem to follow from these considerations which would challenge the underlying assumption that tremors leading to rockburst events are caused by a fracturing of the roof strata. From the standpoint of geomechanics, this process should occur when the critical effort state should arise in the specified zone within the rock strata; the critical effort being the function of the stress–strain characteristics and strength parameters of the rock medium. In the case analysed here, it will be the burst-prone anhydrite layer. The Coulomb–Mohr failure criterion recalled in the analysis relies on the effort factor (Ω), expressed in terms of the function of elastic strain energy components in the rock strata (A_f, A_v, A_c) and is defined as [44–46]

$$\Omega = \frac{3E_s}{(1+\nu_s)R_cR_r}A_f + sign(\sigma_x+\sigma_y+\sigma_z)\frac{R_c-R_r}{R_cR_r}\sqrt{\frac{6E_s}{(1-2\nu_s)}A_v} \quad (1)$$

$$A_f = \frac{1+\nu_s}{6E_s}\left[(\sigma_x-\sigma_y)^2+(\sigma_y-\sigma_z)^2+(\sigma_z-\sigma_x)^2+6\left(\tau_{xy}^2+\tau_{zx}^2+\tau_{yz}^2\right)\right] \quad (2)$$

$$A_v = \frac{1-2\nu_s}{6E_s}(\sigma_x+\sigma_y+\sigma_z)^2 \quad (3)$$

$$A_c = \frac{1}{2E_s}\left[\sigma_x^2+\sigma_y^2+\sigma_z^2-2\nu_s(\sigma_x\sigma_y+\sigma_y\sigma_z+\sigma_z\sigma_x)+2(1+\nu_s)\left(\tau_{xy}^2+\tau_{zx}^2+\tau_{yz}^2\right)\right] \quad (4)$$

where

A_f, A_v, A_c—elastic strain energy density (shear A_f, volumetric A_v and total strain energy density, respectively) in the secondary state of stress, J/m^3,
σ_i, τ_{ij}—secondary stress tensor components ($i, j = x, y, z$), Pa,
R_c, R_r—instantaneous compressive and tensile strength, Pa,
E_s, ν_s—Young modulus and Poisson ratio of the medium, Pa, –.

Assuming the ultimate effort to be equal to all physical and structural processes within the material during the induced deformation (under the generalised loads), the formula can be recalled that defines the quoted effort factor in terms of possible values obtained in assessments. As the densities of elastic strain energy components are positively defined (alongside geomechanical parameters), two cases can be distinguished. When $-1 < \Omega < 1$, then the actual effort in the analysed section of the rock strata is less than the critical value and the structural failure will not occur. When $\Omega \geq 1$ or $\Omega \leq -1$, then effort in the considered strata exceeds the critical value, the failure process (fracturing) will be initiated and a tremor is likely to occur.

To analyse the stress–strain characteristics of burst-prone strata in the context of seismic events registered in Year 3 and Year 6, a numerical procedure was applied, based on the following assumptions:

- It was assumed that fracturing (failure) took place on the horizon level of the contact zone between the dolomite and anhydrite layers (Figure 1); this level appears to be most likely in terms of the pre-supposed error in locating the vertical coordinate of registered high-energy events;
- We were cognisant of the state and progress of mining operations at the time when the two events were registered (December in Year 3—Figure 2 and in December Year 6—Figure 3), and of impacts produced by advancing panelling works, liquidation of working zones and the presence of the existing gobs and development openings in neighbouring plots, as well as the applied methods of roof control (deflection, backfilling);
- The presence of faults with relatively low downthrow (in relation to the height of the face entry drivage) and their impacts on the state of stress within the burst-prone layer were neglected; hence, the lower value of the derived safety factor in regions in the vicinity of faults, characterised by the presence of additional stress concentration zones and areas of elastic strain energy concentration,
- The effects of potential changes in the structure of burst-prone formations (and consequent changes in their geomechanical properties) due to previous mining-induced seismicity were neglected; a quantitative analysis of such changes is in fact not feasible.

3. Results and Discussion

Based upon the theoretical underpinnings and initial assumptions, the numerical procedure was applied to model the mining conditions in panel XVII/1 as of the dates the two rockbursts of concern were studied. In the case of the first event (end of Year 3), the area of concern is indicated in Figure 2 outlined with the red line (area of concern #1), in the case of the other rockburst (end of Year 6), it is likewise shown in Figure 3 (area of concern #2). Simulation results are compiled and presented in the form of contour maps and characteristic ranges (sketched in colours) of the variability distribution patterns:

- Shear strain energy density factor ($k(A_f)$) on the level of burst-prone layers of the main roof (the dolomite–anhydrite interface), defined as

$$k\left(A_f\right) = \frac{A_f}{A_f^{grav}} \tag{5}$$

  where A_f^{grav}—density of the primary shear strain energy associated with gravity-induced stress exclusively, J/m^3.
- Effort factor (Ω) related to the same roof horizon, –.

Actually, all assessments of mining-induced behaviour of rock strata can rely on broader analyses, exploring the stress/strain behaviour, displacement and strain elastic energy or effort parameters. In consideration of the underlying objectives of the study and the adopted synthetic approach, the analysis was restricted to two relatively universal parameters. Strain energy density and effort allow for coupling the deformation and stress-related parameters to mechanical properties of rocks. In relation to the elastic strain energy, the scope of the present study was limited to analyses of the component associated with shear strain as a more reliable indicator in consideration of the subject matter of the study. According to energy-effort criteria [47], the measure of effort is assumed to be the shear strain elastic energy density plus a fraction of volumetric strain energy. Pertinent results obtained for the mining conditions at the end of Year 3 (Figure 2) are shown in Figure 6 ($k(A_f)$) and in Figure 7 (Ω); those relevant to the conditions at the end of Year 6 (Figure 3) are given in Figure 8 ($k(A_f)$) and Figure 9 (Ω). Each of the contour maps reveal the locations of rockburst events in the energy class in excess of 10^4 J (Figures 6 and 7—covering the period of the first three years of mining operations, Figures 8 and 9—Year 6). For better clarity,

the respective ranges of analysed parameters and the energy classes of registered events are referenced in the legend. The presence of a tremor of 10^9 J shown in Figures 6 and 7 merits an explanation as it was not included in earlier statistics (Table 2). The established location of its focus is correct yet the tremor occurred in consequence of mining activities in the neighbouring panel, before working panel XVII/1.

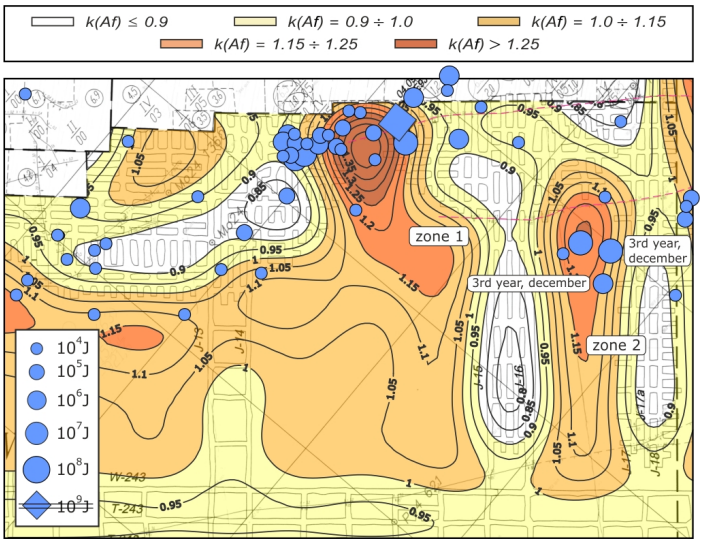


Figure 6. Shear strain energy density (end of Year 3).

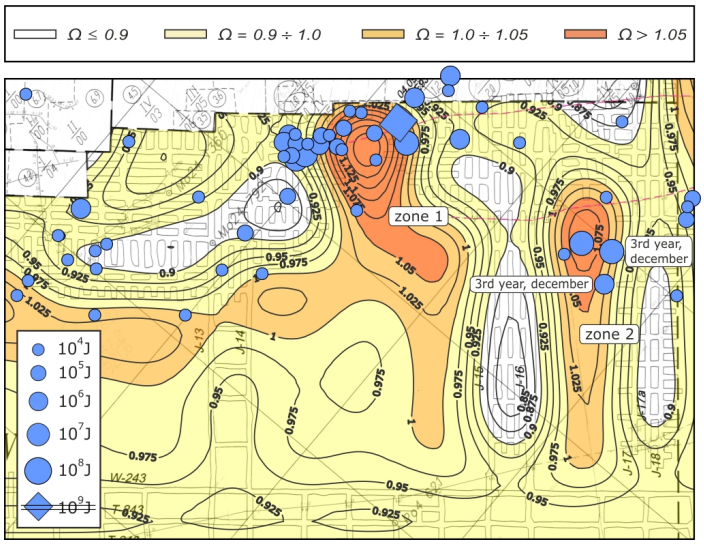


Figure 7. Effort factor (end of Year 3).

A rigorous analysis of shear strain energy density factor ($k(A_f)$) and effort factor (Ω) distributions reveals that the variability ranges for the analysed events (in Year 3 and Year 6) are similar. It is reasonable to conclude, therefore, that potentially burst-prone roof formations (including the anhydrite layer) were subject to strong deformations, which is evidenced by the gradients of investigated parameters, particularly in the case of the first event (Figures 6 and 7). It should be assumed that the current state of deformation of the main roof must be the consequence of extensive mining activities in the neighbouring panels alongside panel XVII/1. The zones of shear strain energy density concentration and those of maximal effort are irregular and are basically found in two distinct areas, each overlying the undisturbed ore body:

– For the mining conditions as of Year 3 (Figures 6 and 7): on the left-hand side of the advancing face, near the old workings, between the descending galleries J-13/14 and J-15/16 (zone 1) and in the vicinity of development openings in between the descending galleries J-15/16 and J-17/18 (zone 2);
– For the mining conditions as of Year 6 (Figures 8 and 9): on both sides of the advancing face alongside the development openings separated by a cluster of galleries T,W-243, between the panelling line and the descending galleries J-13/14 and J-15/16 (zone 1, zone 2).

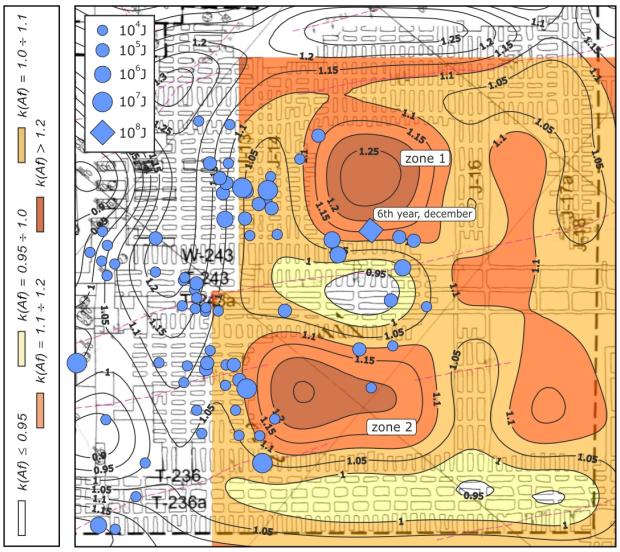


Figure 8. Shear strain energy density (end of Year 6).

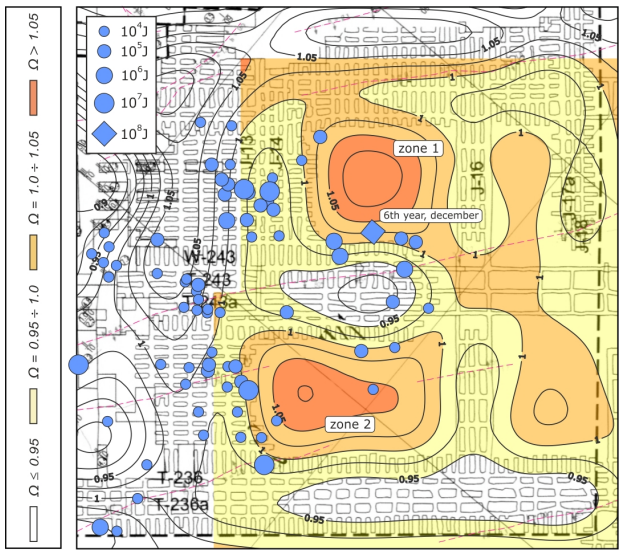


Figure 9. Effort factor (end of Year 6).

The fact that the extreme values of elastic strain energy density and of the effort factor are registered over the undisturbed orebody seems unchallenged, chiefly on account of the tensile nature of horizontal stresses. On the other hand, there may be some discrepancies in interpretations of seismicity assessments and analyses (especially in regard to high-energy events). The graphical representation of the maximum-value zones (zone 1, zone 2) will only roughly correspond with graphed foci locations of tremors registered in December in Year 3 (Figures 6 and 7) and in December in Year 6 (Figures 8 and 9). Simulation results covering the moment when the first rockburst occurred reveal the presence of the

maximum-value zones in between the descending galleries J-13/14 and J-15/16 (zone 1) whilst the epicentre of the tremor of 5.1×10^7 J (followed by an aftershock of 1.3×10^6 J) was registered in between the galleries J-15/16 and J-17/18 (zone 2 in Figure 6).

This state of affairs can possibly be explained in the light of the underlying assumptions whereby seismic activity prior to the rockbursts and its effects on the structure and elastic properties of roof strata should be neglected in numerical simulations. One has to bear in mind that prior to the impact-exerting rockburst, some seismic activity would be already registered in the area, revealed by a number of seismic events in a full range of energies, including the events in the energy class $\geq 10^7$ J (Table 2). The effects that high-energy tremors have on rock formations lead to microcracking and rock fracturing, and, consequently, to the weakening of burst-prone strata causing the change of their geomechanical parameters. Recalling the mechanics of deformable bodies, it can be demonstrated that the amount of elastic strain energy accumulated in a fractured medium (a part of which will be released during the fracturing process) should be less than energy accumulated in a fracture-free rock. That is why the elastic strain energy density and the effort values derived for zones overlying the undisturbed rock body might be overestimated. In consequence, in terms of energy release, the main roof at numerically modelled zones might not be able to handle a high-energy tremor. What is more, neglecting the effects of faults with small downthrow might produce reverse effects (i.e., locally underestimated values of respective indices). In the case of tectonic disturbances adjoining the burst-prone layer, there are still unrelieved stresses (and energy changes) due to primary rock deformation. Notwithstanding, the forecasts being developed allow us to draw conclusions at least in qualitative terms, considering that the available set of data on geomechanical parameters of the rock strata is yet limited. Results of the analytical assessment carried out for two considered cases (i.e., mining conditions at the end of Year 3 and Year 6) have revealed the local zones in roof formations above the orebody horizon which are subject to the complex and most unfavourable state of stress. These analyses suggest that high-energy tremors in the energy class 5.1×10^7 J (end of Year 3) and 1.5×10^8 J (end of Year 6) might have been caused by failure of strongly deformed main roof layers.

Applications of the forecasting method resulted in formulating recommendations as to further mining operations in panel XVII/1, following the second rockburst event. In Section 2.2 relating to the seismic activity, the hypothesis was formulated stating that a considerable reduction of seismic risk (and the risk of the next rockburst occurrence) during continuing mining operations was unlikely as long as the same mining methods were employed. In consideration of workers' safety, certain modifications were necessary in order to reduce mining-induced seismicity, particularly in the high-energy range. Assuming that the registered seismic activity could be attributable to activation of burst-prone main roof formations caused by deformations to their original structure, it is reasonable, therefore, to seek solutions aimed to limit the extent of roof deformation in the course of future mining works. It was established that the major determinants of future roof deformation in the analysed panel include the following:

- Vertical roof displacement (deflection) over the development openings and old excavations;
- Areas opened by panelling works in the orebody.

In regard to the first aspect (i.e., roof deflection), it is suggested that the roof control method be changed and the hydraulic filling be employed regardless of the actual height of the face entry drivage and system requirements. The other aspect (presence of openings) is associated with intensity of mining operations, being the function of the rate of face advance and its length. As reducing the rate of face advance (to date it is ~15 m/month) might enhance the risk of roof caving, it was suggested that the face range be shorter. Along the cluster of galleries T,W-243 the panel is divided into two sections (blocks A and B) in which the operations should progress sequentially, starting from section A abutting on the old excavation on the left-hand side (Figure 3). The elements that should positively reduce the exposed roof area are the width of the opening size, expressed as the distance between

the working faces in the panelling and in liquidation works. Additional simulations were performed to highlight the distribution of the shear strain elastic energy density in the burst-prone strata in the function of the variable development opening size (Figure 10). The results were obtained for the cross-profile A–B located in the axis of the A block and are related to the mining conditions when the mining operations are re-commenced (in accordance with recommendations quoted in the previous section) and the rate of face advance should be 50 m. The reference plot (black coloured, Figure 10) depicts the conditions prior to the rockburst event (in Year 6), when the average width of the opening size was ~270 m; the remaining plots reveal the gradual decrease in this parameter, down to 200, 150 and 100 m.

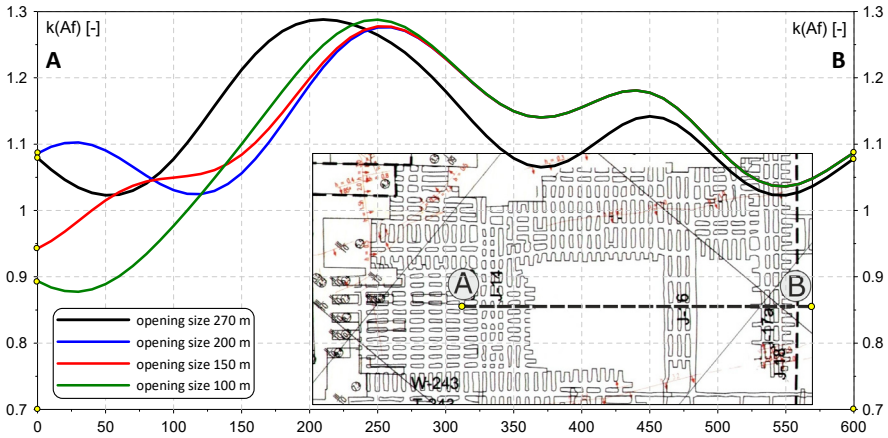


Figure 10. Shear strain energy density along the+ cross-profile A–B.

It is readily apparent that variability of the energy density factor expressed as its maximum values over the undisturbed rock body related to variable width of the opening size is relatively small. However, on account of major fluctuations observed in the development zone, it is suggested that appropriate distance should be maintained between the panelling lines and liquidation works, not exceeding the minimum value (150–170 m) necessary for the mining processes.

These recommendations were implemented and, from the time perspective, were found to be merited producing the desired results. From the year when mining operations were resumed (Year 7) until the end of panelling works in block A within the panel XVII/1 (Year 10), the registered mining-induced seismicity (Table 3) was significantly lower than in the last 6 years (Table 2).

Table 3. Mining-induced seismicity in panel XVII/1 (registered in 4 subsequent years).

Year	10^3 J	10^4 J	10^5 J	10^6 J	10^7 J	10^8 J	ΣN [–]	ΣE [J]	$\Sigma E_w/N_w$ [J]
7th	29	14	5	6	1	--	55	4.71×10^7	3.87×10^6
8th	27	6	1	2	--	--	36	1.50×10^7	4.93×10^6
9th	38	15	--	2	--	--	55	5.46×10^6	2.45×10^6
10th	36	13	7	3	--	--	59	7.29×10^6	6.72×10^5
Σ/av.	130	48	13	13	1	--	205	7.49×10^7	2.70×10^6

During the 4-year period, 205 tremors were registered with energy $\geq 10^3$ J (including 13.1% of events in the energy class $\geq 10^5$ J), with the energy released totalling 7.49×10^7 J (including 97.3% of events in the energy class $\geq 10^5$ J). The year-average of tremors in the energy class $\geq 10^3$ J is ~51/year (a 79.7% decrease), including the population of high-energy tremors ($\geq 10^5$ J), with the year-average ~7/year (a decrease by 82.9%). In terms of energy

range, the year-averaged energy released by the rock strata after the resumption of mining works remained at the level of ~1.87×10^7 J/year, showing a 92.3% decrease in relation to the earlier periods. The average amount of energy released per single high-energy tremor was reduced by half (2.70×10^6 J vs. 5.89×10^6 J). Regarding impact-exerting seismic events, only one de-stressing event was registered in the excavations (Year 7) and it occurred during the delay time after blasting, when the crew were absent.

4. Conclusions

The study recapitulates and synthesises the results of predictions using the energy density and effort factor to explore the rockburst and seismic hazard in panel XVII/1 in the copper mine Rudna. The main objective was the back-analysis of the potentials of activating burst-prone layers in the main roof formations to highlight the origins and underlying causes of two registered rockbursts triggered by high-energy tremors. The provided analyses leads us to the following conclusions:

(a) The level of mining-induced seismicity during the mining operations was relatively high, showing a gradual increase in quantitative terms, revealing cyclical fluctuations in terms of energy release. Registered rockbursts were triggered by strong tremors whose epicentres were, to a large extent, located in the vicinity of the gob boundary and development works; only in a few cases were they located in the neighbourhood of tectonic faults of small downthrow.

(b) At the time the two analysed rockbursts occurred, the main roof layers with a high rockbursting potential (including the anhydrite layers) were strongly deformed as a result of mining of the adjoining panels and due to the presence of vast areas of development openings and splitting pillars within the working zone in panel XVII/1. Furthermore, the structure of burst-prone formations might have been disturbed by dynamic interactions due to previous mining-induced seismicity, particularly high-energy seismic events.

(c) The zones of shear strain elastic energy density concentration and maximal values of the effort factor derived by numerical modelling are located on the face range, encompassing the areas overlying the uncut sections of the orebody adjacent to old excavations and development sites.

(d) The result of the back analysis and predictions have confirmed that the state of stress and strain in roof strata was nonuniform, locally most unfavourable. In the context of mining-induced seismicity, the anomaly zones in graphic representation would correspond with locations of epicentres of rockburst-triggering tremors.

(e) The two high-energy rockburst events in the energy class of 5.1×10^7 J and 1.5×10^8 J can presumably be attributed to critical efforting of the rock strata due to progressing rock fracturing on the horizon of strongly deformed anhydrite formations. Identification of the underlying causes of these events allowed the plans of further mining operations to be verified accordingly. The implemented technical solutions proved to be justified and produced the desired effects limiting the mining-induced seismicity both in quantitative terms and in terms of energy release.

In sum, it appears that predictions and forecasts underpinned by less complex geomechanical models, when supported by ongoing geophysical observations, can be considered as a reliable source of information about the strata behaviour in the conditions of continuing underground mining operations, and can be effectively used in evaluations of the seismic and rockburst hazard levels. They provide the backgrounds for developing effective measures aimed at an optimal selection of the room and-pillar system components, as well as preventive measures and rockburst control strategies.

Author Contributions: D.C.: research/paper idea, data analysis and verification, stress state analytical modelling, results comparison, conclusions and final editing; Z.B.: data collecting and preliminary analysis, seismicity parameters calculation/processing, results visualisation and draft text editing. All authors have read and agreed to the published version of the manuscript.

Funding: The research was funded by AGH University of Krakow; subsidy numbers 16.16.100.215.

Institutional Review Board Statement: Not applicable.

Informed Consent Statement: Not applicable.

Data Availability Statement: Data are contained within the article.

Conflicts of Interest: The authors declare no conflicts of interest.

References

1. Butra, J.; Mrozek, K.; Osadczuk, T. *Aktualny Stan Zagrożenia Tąpaniami w Kopalniach KGHM Polska Miedź SA. Prace Naukowe Instytutu Geotechniki i Hydrotechniki Politechniki Wrocławskiej (Konferencje)*; Oficyna Wydawnicza Politechniki Wrocławskiej: Wrocław, Poland, 2005; Volume 75, pp. 59–74. (In Polish)
2. Cieślik, J.; Burtan, Z.; Chlebowski, D.; Zorychta, A. Geomechanical analysis of location and conditions for mining-induced tremors in LGOM copper mines. *J. Sustain. Min.* **2017**, *16*, 94–103. [CrossRef]
3. Stec, K. Skala zagrożenia sejsmicznego w Górnośląskim Zagłębiu Węglowym. In *Prace Naukowe GiG (Górnictwo i Środowisko)*; Wydawnictwo Głównego Instytutu Górnictwa: Katowice, Poland, 2007; Volume 3, pp. 55–75. (In Polish)
4. Patyńska, R.; Mirek, A.; Burtan, Z.; Pilecka, E. Rockburst of parameters causing mining disasters in mines of Upper Silesian Coal Basin. 4th Nationwide Scientific Conference on Engineering-Infrastructure-Mining. *E3S Web Conf.* **2018**, *36*, 1–8. [CrossRef]
5. Knopik, M.; Zuberek, W.; Wojtecki, Ł. Wieloprzyczynowość wysokoenergetycznych wstrząsów górniczych. *Przegląd Górniczy* **2015**, *12*, 12–19. (In Polish)
6. Marcak, H. *Modele Rozwoju Deformacji Górotworu Poprzedzającej Tąpnięcie. Badania Geofizyczne w Kopalniach*; Wydawnictwo Instytutu Gospodarki Surowcami Mineralnymi i Energią PAN: Kraków, Poland, 2001; pp. 49–57. (In Polish)
7. Marcak, H. A geophysical model for the analysis of seismic emissions in the area of rock beam splitting caused by mining operations. In *International Mining Forum 2006. New Technological Solutions in Underground Mining, Proceedings of the 7th International Mining Forum, Wieliczka, Poland, 20–24 February 2006*; Sobczyk, E.J., Kicki, J., Eds.; A.A. Balkema Publishers: London, UK, 2006; pp. 73–86.
8. Idziak, A.; Teper, L.; Zuberek, W. *Sejsmiczność a Tektonika Górnośląskiego Zagłębia Węglowego*; Wydawnictwo Uniwersytetu Śląskiego: Katowice, Poland, 1999. (In Polish)
9. Marcak, H.; Mutke, G. Seismic activation of tectonic stresses by mining. *J. Seismol.* **2013**, *17*, 1139–1148. [CrossRef]
10. Zhou, J.; Li, X.; Mitri, H.S. Evaluation method of rockburst: State-of-the-art literature review. *Tunn. Undergr. Space Technol.* **2018**, *81*, 632–659. [CrossRef]
11. Gibowicz, S.J. Seismicity induced by mining recent research. *Adv. Geophys.* **2009**, *51*, 1–53.
12. Hatherly, P. Overview on the application of geophysics in coal mining. *Int. J. Coal Geol.* **2013**, *114*, 74–84. [CrossRef]
13. Marcak, H. Seismicity in mines due to roof layer bending. *Arch. Min. Sci.* **2012**, *57*, 229–250.
14. Gogolewska, A.; Markowiak, A. Seismic activity and convergence in deep mining field, case study from copper ore mine, SW Poland. In Proceedings of the 28th International Symposium on Mine Planning and Equipment Selection; Topal, E., Ed.; Springer Series in Geomechanics and Geoengineering: Berlin/Heidelberg, Germany, 2019; pp. 508–515.
15. Barański, A.; Drzewiecki, J.; Dubiński, J.; Kabiesz, J.; Konopko, W. *Zasady Stosowania Metody Kompleksowej i Metod Szczegółowych Oceny Stanu Zagrożenia Tapaniami w Kopalniach Wegla Kamiennego*; Wydawnictwo Głównego Instytutu Górnictwa: Katowice, Poland, 2012; pp. 15–38. (In Polish)
16. Das, J.P.; Balasubramaniam, V.R.; Goverdhan, K.; Ganapathy, G.P. Overview of seismic monitoring and assessment of seismic hazard based on a decade of seismic events. In Proceedings of the Conference on Recent Advances in Rock Engineering, Bengaluru, India, 16–18 November 2016; Advances in Engineering Research; Atlantis Press: Amsterdam, The Netherlands, 2016; pp. 557–564.
17. Cianciara, A.; Cianciara, B. The meaning of seismoacoustic emission for estimation of time of mining tremors occurrence. *Arch. Min. Sci.* **2006**, *51*, 563–575.
18. Kornowski, J.; Kurzeja, J. Prediction of rockburst probability given seismic energy and factors defined by the expert method of hazard evaluation (MRG). *Acta Geophys.* **2012**, *60*, 472–486. [CrossRef]
19. Kołodziejczyk, P.; Kornowski, J.; Gołda, I. Zagrożenie sejsmiczne od wstrząsów górniczych w warunkach niepewnej informacji. *Górnictwo I Geol.* **2013**, *8*, 47–60. (In Polish)
20. Stec, K. Focal mechanisms of mine-induced seismic events an explanation of Geomechanical processes in the area of longwall 6, seam 510 in hard coal mine Bobrek-Centrum. *Arch. Min. Sci.* **2012**, *57*, 871–886.
21. Sen, A.T.; Cesca, S.; Bischoff, M.; Meier, T.; Dahm, T. Automated full moment tensor inversion of coal mining-induced seismicity. *Geophys. J. Int.* **2013**, *195*, 1267–1281. [CrossRef]
22. Cao, A.; Liu, Y.; Chen, F.; Hao, Q.; Yang, X.; Wang, C.; Bai, X. Focal Mechanism and Source Parameters Analysis of Mining-Induced Earthquakes Based on Relative Moment Tensor Inversion. *Int. J. Environ. Res. Public Health* **2022**, *19*, 7352. [CrossRef]
23. Mutke, G.; Pierzyna, A.; Barański, A. b-value as a criterion for the evaluation of rock-burst hazard in coal mines. In Proceedings of the 3rd International Symposium on Mine Safety Science and Engineering (ISMS), Montreal, QC, Canada, 13–19 August 2016; pp. 1–5.

24. Wesseloo, J. Addressing misconceptions regarding seismic hazard assessment in mines: B-value, Mmax, and space-time normalization. *J. South. Afr. Inst. Min. Metall.* **2020**, *120*, 67–80. [CrossRef]
25. Dubiński, J.; Stec, K.; Krupanek, J. Comprehensive use of the Gutenberg–Richter law and geotomography for improving seismic hazard evaluation in hard coal mines. *Int. J. Coal Sci. Technol.* **2023**, *10*, 3. [CrossRef]
26. Hosseini, N. Evaluation of the rockburst potential in longwall coal mining using passive seismic velocity tomography and image subtraction technique. *J. Seismol.* **2017**, *21*, 1101–1110. [CrossRef]
27. Ma, X.; Westman, E.; Malek, F.; Yao, M. Stress redistribution monitoring using passive seismic tomography at a deep nickel mine. *Rock Mech. Rock Eng.* **2019**, *52*, 3909–3919. [CrossRef]
28. Mutke, G.; Dubiński, J.; Lurka, A. New criteria to assess seismic and rockburst hazard in coal mines. *Arch. Min. Sci.* **2015**, *60*, 743–760.
29. Zhang, W.; Ma, N.; Ren, J.; Li, C. Peak particle velocity of vibration events in underground coal mine and their caused stress increment. *Measurement* **2021**, *169*, 108520. [CrossRef]
30. Lasocki, S.; Orlecka-Sikora, B. Seismic hazard assessment under complex source size distribution of mining-induced seismicity. *Tectonophysics* **2008**, *456*, 28–37. [CrossRef]
31. Wesseloo, J. The spatial assessment of the current seismic hazard state for hard rock underground mines. *Rock Mech. Rock Eng.* **2018**, *51*, 1839–1862. [CrossRef]
32. Pu, Y.; Apel, D.B.; Liu, V.; Mitri, H. Machine learning methods for rockburst prediction-state-of-the-art review. *Int. J. Min. Sci. Technol.* **2019**, *29*, 565–570. [CrossRef]
33. Cichy, T.; Prusek, S.; Świątek, J.; Apel, D.B.; Pu, Y. Use of neural networks to forecast seismic hazard expressed by number of tremors per unit of surface. *Pure Appl. Geophys.* **2020**, *177*, 5713–5722. [CrossRef]
34. Kabiesz, J.; Makówka, J. Selected elements of rock burst state assessment in case studies from the silesian hard coal mines. *Min. Sci. Technol.* **2009**, *19*, 660–667. [CrossRef]
35. Lin'kov, A.M. Numerical modeling of seismic and aseismatic events in geomechanics. *J. Min. Sci.* **2005**, *41*, 14–26. [CrossRef]
36. Pytel, W.; Mertuszka, P.; Jones, T.; Paprocki, H. Numerical simulations of geomechanical state of rock mass prior to seismic events occurrence—Case study from a Polish Copper Mine aided by FEM 3D approach. In Proceedings of the 27th International Symposium on Mine Planning and Equipment Selection; Widzyk-Capehart, E., Hekmat, A., Singhal, R., Eds.; Springer: Berlin/Heidelberg, Germany, 2018; pp. 417–427.
37. Małkowski, P.; Niedbalski, Z. A comprehensive geomechanical method for the assessment of rockburst hazards in underground mining. *Int. J. Min. Sci. Technol.* **2020**, *30*, 345–355. [CrossRef]
38. Dymek, F. Przemieszczeniowe zadanie brzegowe przestrzennej teorii sprężystości i jego zastosowanie do zagadnień mechaniki górotworu. *Arch. Min. Sci.* 1969; XIV, 263–280. (In Polish)
39. Gil, H. *The Theory of Strata Mechanics*; Wydawnictwo PWN: Warszawa, Poland, 1991.
40. Ozog, T. *Ugięcie Stropu Przy Uwzględnieniu Sił Ścinających*; Zeszyty Problemowe Górnictwa PAN: Kraków, Poland, 1965; Volume 3, pp. 45–79. (In Polish)
41. Budryk, W. Stan naprężeń w górotworze pod wpływem wyeksploatowania pokładu. *Arch. Górnictwa I Hut.* **1955**, *4*, 90–102. (In Polish)
42. Sałustowicz, A. *Zarys Mechaniki Górotworu*; Wydawnictwo Śląsk: Katowice, Poland, 1968. (In Polish)
43. Knothe, S. *Prognozowanie Wpływów Eksploatacji Górniczej*; Wydawnictwo Śląsk: Katowice, Poland, 1984. (In Polish)
44. Sih, G.C. Methods of analysis and solutions of crack problems. Recent developments in fracture mechanics. Theory and methods of solving crack problems. In *Mechanics of Fracture*; Noordhoff International Publishing: Leyden, IL, USA, 1973; Volume 1.
45. Kłeczek, Z. *Geomechanika Górnicza*; Wydawnictwo AGH: Warszawa, Poland, 1985; no 1000. (In Polish)
46. Chlebowski, D. *Energetyczna Ocena Możliwości Wystąpienia Procesów Pękania w Utworach Anhydrytowych na Przykładzie Oddziału G-22 O/ZG Rudna. Prace Naukowe GiG (Górnictwo i Środowisko)*; Wydawnictwo Głównego Instytutu Górnictwa: Katowice, Poland, 2011; Volume 4, pp. 43–51. (In Polish)
47. Szeptyński, P. Some remarks on Burzyński's failure criterion for anisotropic materials. *Eng. Trans.* **2011**, *59*, 119–136.

Disclaimer/Publisher's Note: The statements, opinions and data contained in all publications are solely those of the individual author(s) and contributor(s) and not of MDPI and/or the editor(s). MDPI and/or the editor(s) disclaim responsibility for any injury to people or property resulting from any ideas, methods, instructions or products referred to in the content.